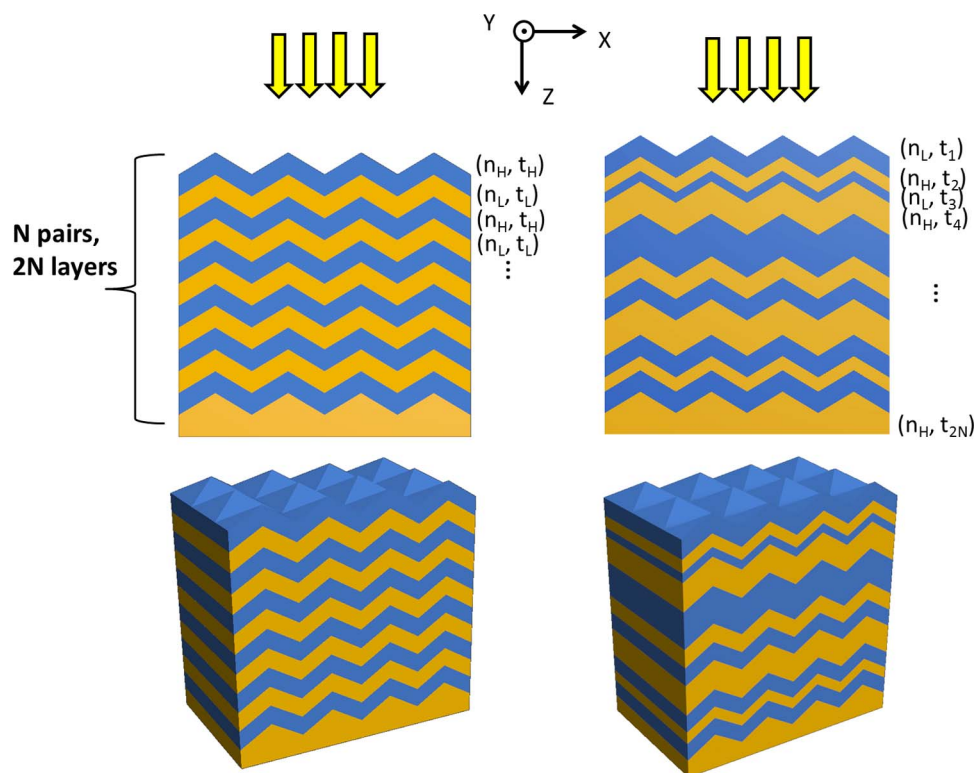


Arbitrarily-Wide-Band Dielectric Mirrors and Their Applications to SiGe Solar Cells

Volume 7, Number 4, August 2015

Yan Kai Zhong
Sze Ming Fu
Sheng Lun Yan
Po Yu Chen
Albert Lin



DOI: 10.1109/JPHOT.2015.2452771
1943-0655 © 2015 IEEE

Arbitrarily-Wide-Band Dielectric Mirrors and Their Applications to SiGe Solar Cells

Yan Kai Zhong, Sze Ming Fu, Sheng Lun Yan, Po Yu Chen, and Albert Lin

Department of Electronic Engineering, National Chiao Tung University, Hsinchu 30010, Taiwan

DOI: 10.1109/JPHOT.2015.2452771

1943-0655 © 2015 IEEE. Translations and content mining are permitted for academic research only.

Personal use is also permitted, but republication/redistribution requires IEEE permission.

See http://www.ieee.org/publications_standards/publications/rights/index.html for more information.

Manuscript received June 8, 2015; revised June 28, 2015; accepted June 30, 2015. Date of publication July 2, 2015; date of current version July 13, 2015. Corresponding author: A. Lin (e-mail: hdt5746@gmail.com).

Abstract: The dielectric mirror is an important optical component for optoelectronic devices, passive photonic devices, and solar cells. Unfortunately, the reflection bandwidth of distributed Bragg reflectors (DBRs) and high-index contrast mirrors (HCGs) are limited by the index contrast of the material system used. Here, an aperiodic design for dielectric mirrors is proposed, and it is shown that for a fixed index contrast, the bandwidth of the reflection band can be arbitrarily widened by simply incorporating more dielectric layers. This is pronouncedly different from the fixed bandwidth of HCGs and DBRs. The physics behind the broadband reflection for the aperiodic stacking is identified as the photonic bandgap widening due to the annihilation of the quasi-guided modes in nonperiodic structures. This observation applies very well to aperiodic auto-cloned 3-D photonic crystal reflectors, to aperiodic DBRs, and even to diffuse dielectric mirrors that have recently emerged to be very promising for solar cells due to their zero plasmonic absorption nature. Experimentally, the white paint diffuse medium reflectors are applied to SiGe solar cells to confirm their high reflectance and the feasibility of enhancing solar cell efficiency.

Index Terms: Subwavelength structures, nanostructures, photovoltaics, photonic band-gap structure, diffractive optics.

1. Introduction

Dielectric mirrors are of particular interest for photonic and optoelectronic applications due to their higher reflectance and zero metallic absorption loss compared to metal reflectors. For solar cells, the dielectric mirrors can potentially provide low-cost, high throughput, and zero plasmonic absorption loss alternatives to metallic mirrors. The wide range of process temperature is also an attractive characteristic for the dielectric mirrors. For example, the higher process temperature for distributed Bragg reflectors is beneficial for integrating into optoelectronic devices or circuits such as a vertical cavity surface emitting laser (VCSEL) [1]. On the other hand, low cost, low process temperature, printing-compatible, and zero plasmonic absorption white paint diffuse mirrors have been emerging as an alternative to metallic back reflectors [2], [3] for photovoltaics (PV). The additional advantage of dielectric mirrors is that the tunability of the spectral response can be easily achieved by changing their physical dimensions [4], [5]. This is more difficult for metallic mirrors [6]–[9].

The most-significant drawback of dielectric mirrors is the limited bandwidth. Currently a periodic distributed Bragg reflector (DBR) [1], [10] and a high index contrast grating (HCG) [6], [7],

[11]–[13] can only achieve reflection bandwidth < 200 nm for photovoltaics application spectral range, i.e., 400 nm–1000 nm. In this work, it is shown that the key to increasing the bandwidth for dielectric mirrors is through aperiodic stacking. It will be shown that the reflection bandwidth can be widened for a fixed index contrast ratio using an aperiodic design. This is unachievable by periodic designs using DBRs or HCGs.

First, the physics behind arbitrarily-wide reflection band is revealed by examining the photonic bandstructure using the simplest planar DBR mirrors. The periodic and aperiodic DBR design is carefully examined. The widened reflection band is shown to be the result of the gradual annihilation of quasi-guided modes in an aperiodic structure. Second, aperiodic auto-cloned 3-D photonic crystal reflectors (PCR), diffuse medium reflectors, and distributed Bragg reflectors (DBR) are studied, and the arbitrarily widened reflection bandwidth are observed in all three cases.

2. Calculation Method and Problem Set-up

The calculation method is based on rigorously coupled wave analysis (RCWA) implemented by Rsoft Diffractmod. The polarization angle is 45° and, therefore, the result is the average of s- and p-polarization. In fact, the calculation results are exactly the same for s-, p-, or 45° polarization since the structure is highly symmetric. The refractive index for all of the dielectric mirror structure in this study is $n_H = 2.5$ and $n_L = 1.5$, which can be easily achievable with common dielectric materials such as titanium oxide (TiO_2), silicon nitride (Si_3N_4), silicon dioxide (SiO_2), or various organic polymers. The air-gapped devices can generally provide higher index ratio, but it will be shown here that the insufficient index contrast ratio can be compensated by more stacked layers if an aperiodic design is used. From our point of view, the aperiodicity can be of random or of optimized nature. All of the structures are optimized in part or in all of their geometries. Specifically speaking, for A-PCRs, all of the geometry parameters are optimized by a genetic algorithm (GA) including the layer thickness and the period of auto-cloned deposition. For aperiodic diffuse medium reflectors, the scatterer dimension and horizontal spacing are optimized by GA. The vertical spacing is randomly selected to simulate the scenario in real white paint reflectors. The reason that the randomly selected horizontal spacing cannot be employed is stated in the next paragraph. For A-DBRs, since the problem is simpler by itself, iterative runs are conducted, and a wideband individual is selected. GA is not necessary in the case of A-DBRs.

For diffuse medium mirrors, several solution process techniques can lead to ordered dielectric scatterers embedded in background low index host materials [14], [15]. Nonetheless, the randomly distributed scatterers will be shown to be capable of providing significantly greater bandwidth. Previously, different approximated solution methods for Maxwell's equations, including a Monte Carlo method [16], N -flux methods based on radiation transfer equations [17]–[19], and an 1-D approximation based on semi-coherent optical modeling [2], have been applied to analyze a diffuse medium. The reflectance in the reflection band is around 80% based on these previous studies. In this work, a more accurate solution method based on RCWA is employed to provide deeper insight into this very promising candidate for solar cell back reflectors. Similar to one-dimensional approximation based on semi-coherent optical modeling in [2], the randomness of dielectric scatterers is only in the propagation direction (normal to the substrate) in the calculation here. The random distribution of dielectric scatterers in all of the three directions is technically impossible to simulate due to the limitation of current CPU and memory upper limit. By the comparison between the random and periodic diffuse mirrors in Section 5, the reflection band is expected to be further widened by the randomization in all of the three directions. Based on this study, it is found that the reflectance in the reflection band can be as high as $> 99\%$, different from previous studies [2], [16]–[19]. In addition, we show that the randomization in scatterer distribution is important for achieving ultrabroadband response for diffuse medium mirrors. Undoubtedly, if the scatterer distribution is optimized aperiodically, its bandwidth can be even wider than the random ones. Nonetheless, unlike A-PCRs or A-DBRs, optimized aperiodicity is more difficult to achieve in the case of diffuse mirrors.

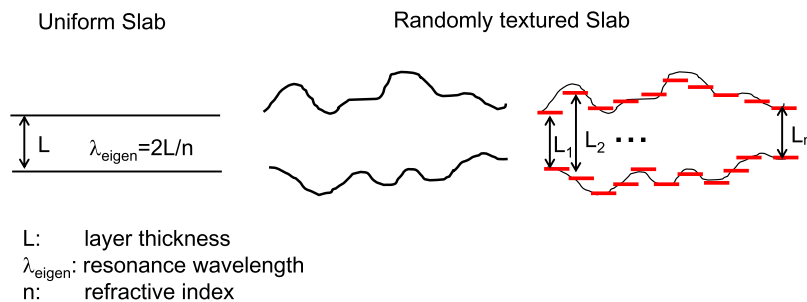


Fig. 1. Blurring of the resonance condition in a randomized structure. The L is the layer thickness of the dielectric slab. In the case of a uniform thickness (L) dielectric slab, the Fabry–Perot resonance condition is unambiguously $\lambda_{\text{eigen}} = 2L/n$, where n is the refractive index of the dielectric. In the case of a randomly textured dielectric slab, the thickness of the slab varies locally, and they are denoted by L_1, L_2, \dots, L_n . The resonance wavelength becomes blurred due to the varied thickness in the random structure.

The target response wavelength is chosen to be 400 nm to 1000 nm in this study, which is suitable for silicon PV applications. It can be easily scaled to other wavelengths due to the decent scalability of dielectric mirrors. In the cases of A-PCRs and diffuse medium reflectors, the genetic algorithm (GA) is employed for locating the optimal geometries for a broadband reflectance. GA is chosen due to the fact that it does not require initial guesses. A genetic algorithm (GA) or an evolutionary algorithm is a stochastic global search method that mimics the metaphor of natural biological evolution [20]. The principle of survival of the fittest is applied to a population of individuals, which are potential solutions to the problem. Individuals with higher fitness in the problem domain have a better chance to be selected and to reproduce their own offspring. Genetic algorithms are particularly suited for search in very large or unbounded sample spaces, and it has been proven useful in many different fields [21]–[24].

3. Physics for Arbitrarily-Wide-Band Using Aperiodic Stacking: Photonic Bandgap Widening

In general, the quasi-guided modes excitations in a dielectric mirror will lead to the reflectance dips due to the coupling of the incident wave into the Bloch propagation modes of the mirror structure. One important thing is to distinguish this mode coupling in dielectric mirrors from the mode coupling in solar cells. In solar cells, the reflector is only part of the entire device structure, which typically consists of an anti-reflection coating, an absorber, a dielectric spacer if necessary, and then a back reflector. Therefore, along the line of the terminology in solar cell optics, the coupling into Bloch modes is usually referring to the coupling to the Bloch modes propagating in the absorber layer. Here, only mirror structures are considered, so when the optical mode is mentioned, it is referred to the propagating modes in the dielectric mirrors itself. This point is explained quite well in [25]. As a result, if the incidence wave is coupled into the optical modes associated with the dielectric mirror, high reflectance will disappear.

For periodic structures, the interference and resonance phenomenon is more pronounced due to their well-defined geometry. On the other hand, for the aperiodic or randomized structures, the guided mode peaks will generally become broader, which has been observed for solar cells [26], [27]. In the literature of the solar cells with a randomly textured front or rear surface, it is reported that the absorption peak will become less pronounced compared to their periodic counterparts. The physics is illustrated in Fig. 1. For a well-defined dielectric slab, the resonance conditions are clear and therefore at the resonance wavelengths, the guided modes are excited. On the other hand, for randomized or aperiodic structures, the resonance condition is blurred by the aperiodic or randomized geometry, and this generally results in spectral linewidth broadening.

Using the simplest example, i.e., random layer thickness DBR, the phenomenon can be further illustrated by observing its gradually reduced resonance strength as the randomization in

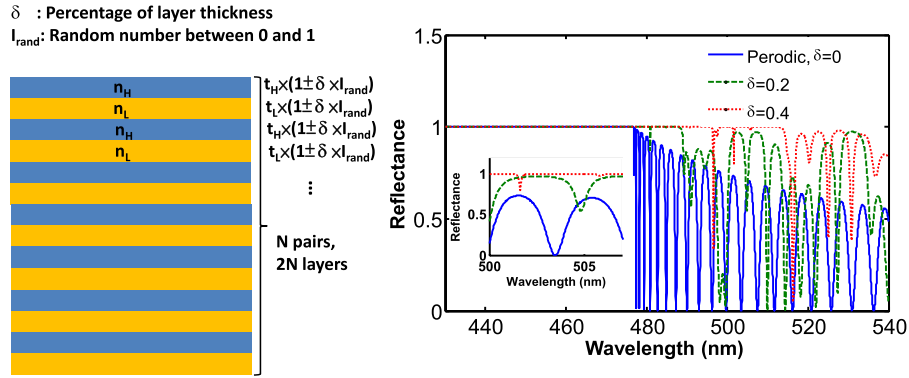


Fig. 2. Gradual annihilation of quasi-guided modes in the DBR structure if the randomness in layer thickness is increased. n_H and t_H are the refractive index and the thickness of the high index material. n_L and t_L are the refractive index and the thickness of the low index material. The percentage of randomness is defined as the fraction of the layer thickness that is randomly determined. $N = 100$.

Photonic Bandstructure above light cone (Reflectance plot)

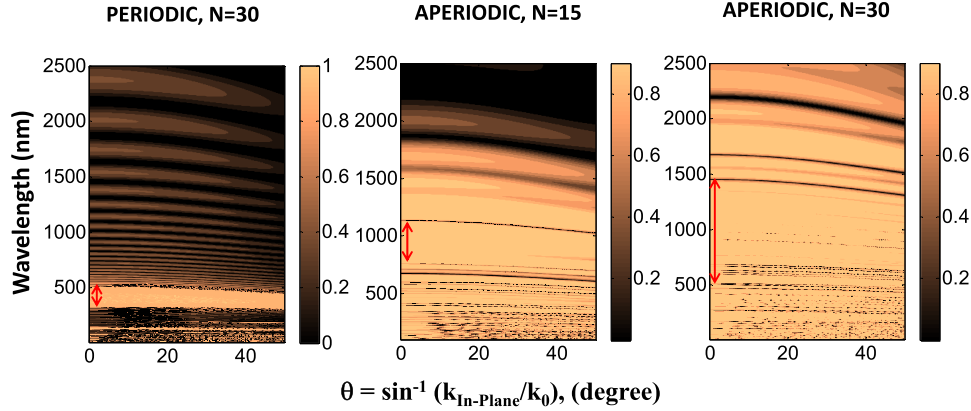


Fig. 3. Photonic band structures for (left) a periodic DBR with pair number $N = 30$, (center) an aperiodic DBR with pair number $N = 15$, (right) an aperiodic DBR with pair number $N = 30$. The photonic bandstructure above the light cone is constructed by calculating reflectance versus wavelength for varying incidence angles, for the DBR and the A-DBRs. The high reflectance zone corresponds to a photonic bandgap (PBG), where the propagation of the Bloch mode is prohibited. The in-plane Bloch wavevectors and the incidence angle θ assume the relation $k_{in-plane} = k_0 \sin\theta$.

its layer thickness becomes greater in Fig. 2. Originally, when the layer thickness is quarter-wavelength centered at 400 nm and $N = 100$, significant reflection dips are observed at some wavelengths. This indicates the coupling into the Bloch modes in the periodic DBR structure. When the randomness in the layer thickness is increased by increasing the percentage of uncertainty, as illustrated in Fig. 1, the quality factor of the reflection dips begins to drop. The percentage of randomness is defined as the fraction of the total thickness of each layer that is randomly determined. The photonic bandstructures is shown in Fig. 3. The reflectance is firstly calculated for different wavelengths and different incident angles. The bandstructure is then constructed by plotting the reflectance versus wavelength (y-axis) and incident angle (x-axis). In Fig. 3, the photonic bandgap (PBG) is determined by the wavelength spacing between the two prominent quasi-guided mode dips. The dips correspond to low reflectance and will appear in black color in the contour plots. The 1-D cut at normal incidence ($\theta = 0^\circ$) for these contour plots is helpful in determining the wavelength spacing between the adjacent two quasi-guided mode dips. It is clearly seen the photonic bandgap widening for the aperiodic structures. On the

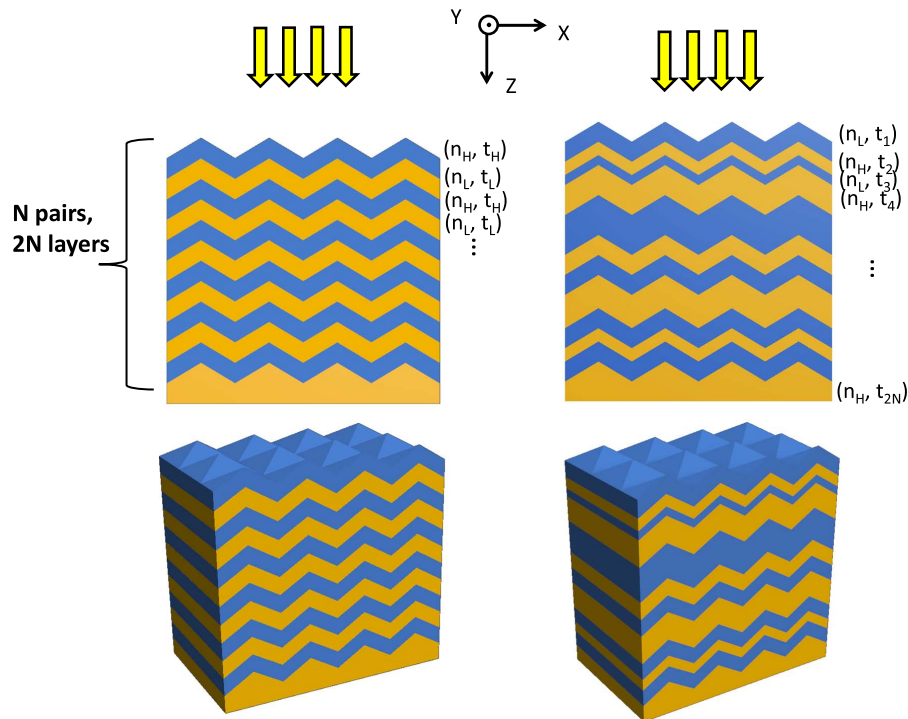


Fig. 4. Three-dimensional auto-cloned photonic crystal reflectors. The drawing here is x - z cross section. The y - z cross section assumes the same profile. The structure is 3-D and polarization independent. (Left) Periodic stacking. (Right) Aperiodic stacking. n_H and t_H are the refractive index and the thickness of the high index material. n_L and t_L are the refractive index and the thickness of the low index material. In the case of aperiodic stacks, the thickness is different for each layer, and it is denoted by t_1, t_2, t_3, \dots , or t_{2N} .

left side of Fig. 3, the photonic band structure for periodic DBR with $N = 30$ is plotted where the bandgap corresponds to the high reflection zone in its spectral response. In the center of Fig. 3, the quasi-guided modes, which corresponds to a black region in the bandstructure plots, begin to blur for the case of A-DBR with pair number $N = 15$. The layer thickness in the case of A-DBR is randomly chosen and ranges from 0 nm to one wavelength. In the right of Fig. 3, the photonic band structure for A-DBR with $N = 30$ is plotted, where it can be seen that the quasi-guided modes are further annihilated resulting even a wider PBG. Therefore, it can be observed that the quasi-guided modes are gradually annihilated with an increased pair number N during the aperiodic stacking. This phenomenon is the key factor contributing to the arbitrarily wide-band reflection using aperiodicity.

Based on the study on A-PCRs, diffuse medium reflectors, and A-DBRs below, it will be clear that the photonic bandgap (PBG), and therefore, the reflection band can be widened arbitrarily with an increased number of stacking pairs. For the ultimate PBG widening limit, it comes from the situation where the layer thickness becomes much smaller than the wavelength. In this scenario, the light scattering by different aperiodic dielectric layers becomes very unpronounced, and the incident wave only sees an effective medium with an effective refractive index that falls between n_H and n_L .

4. Aperiodic Three-Dimensional (3D) Auto-Cloned Photonic Crystal Reflectors (A-PCR)

Auto-cloning is a popular method to fabricate three-dimensional (3D) photonic crystal (PC) as illustrated in Fig. 4. In this process, the simultaneous deposition and etching of alternating materials results in a tapered profile in each deposited layer. Without etching, the tapered profile will

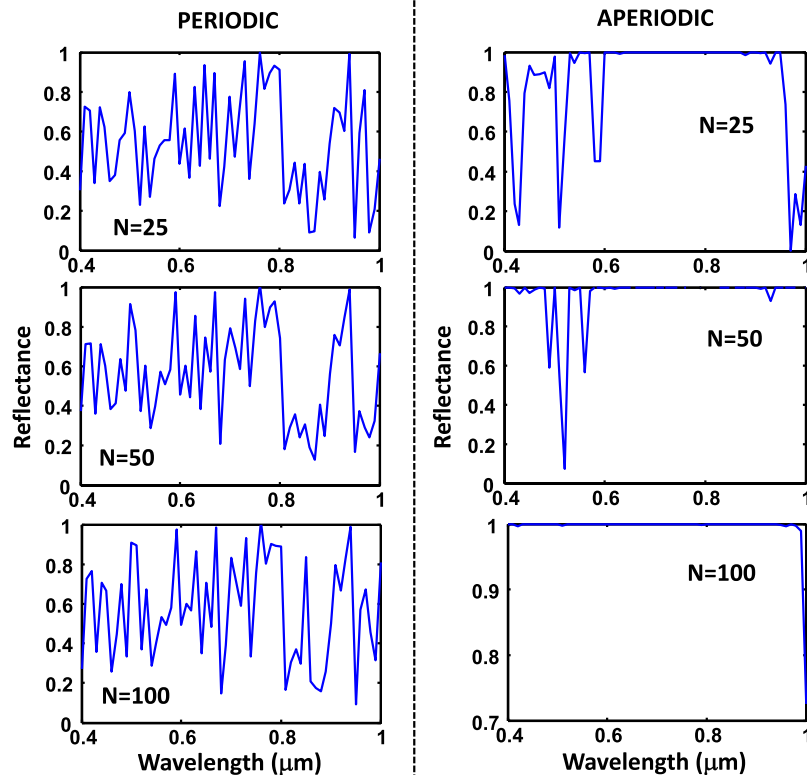


Fig. 5. Spectral reflectance for auto-cloned 3-D PC reflectors. (Left) Periodic stacking. (Right) Aperiodic stacking. The layer thickness and the auto-cloning period are optimized individually by GA. N is the number of pairs.

become more and more smoothened after depositing several layers. The 3-D PC has been shown to be capable of realizing reflectors [28] and filters [29]. Such reflectors have also been incorporated into an optoelectronic device such as light emitting diodes [28]. In order to use it for solar cells, the reflection bandwidth should be further increased to cover the entire solar spectrum. For the periodic PC reflector in Fig. 5, the optimized geometry is $P = 922.8$ nm, $t_L = 289$ nm, and $t_H = 495.1$ nm. For aperiodic PC reflector in Fig. 5, the optimized geometry is $P = 414.2$ nm for $N = 25$, $P = 459.1$ nm for $N = 50$, and $P = 414.2$ nm for $N = 100$. The thickness of each aperiodic layer is not included here due to the fact that it is an extended list. The layer thickness ranges from $0.1 \mu\text{m}$ to $0.5 \mu\text{m}$. It can be seen from Fig. 5 that the periodic 3-D PCR does not show high reflectance if the goal is to cover the 400–1000 nm wavelength range. Increasing the number of layers for periodic PCR does not help to achieve this goal, as evident from Fig. 5. This is attributed to the fact that the periodic structure can only provide definite interference conditions. More periodic PC layers only strengthen this condition but don't change the reflection/transmission behavior. In Fig. 5, aperiodic 3-D PCRs show much wider bandwidth compared to their periodic counterparts. The explanation on the broader bandwidth is due to the annihilation of the quasi-guided modes resulting from the aperiodic stacking. The aperiodic structures in general blur the resonance conditions due to the lack of a fixed and well-defined geometry. This leads to quasi-guided mode annihilation and the photonic bandgap widening. A detailed and in-depth explanation based on the photonic band structure has been presented in Section 3. In Fig. 5, the bandwidth of the aperiodic PCRs can be significantly altered by changing the number of deposited layers, for a given index contrast. This is an extraordinarily promising feature since the bandwidth is unfortunately clamped by the index contrast in periodic designs. While the index contrast is primarily determined by the materials available for a specific application, the aperiodic design relaxes the constraint on the photonic device performance

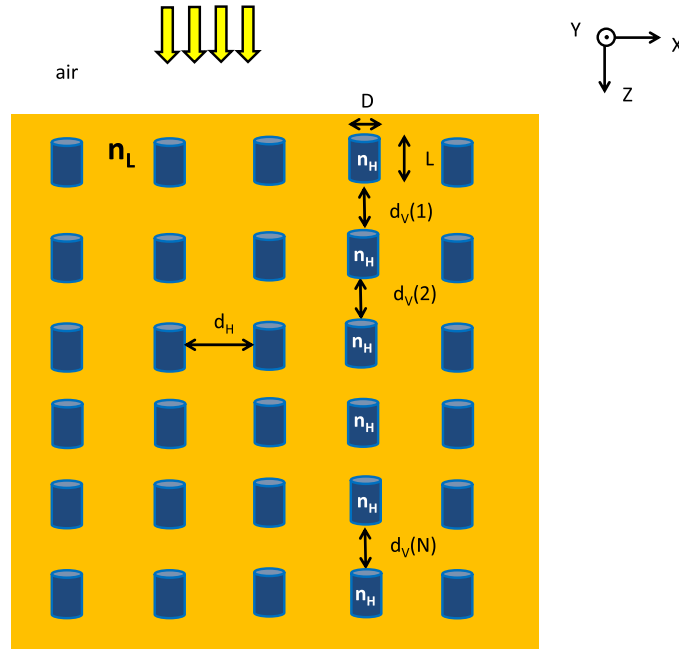


Fig. 6. Diffuse medium reflectors. The distribution of the embedded dielectric scatterers can be random and thus $d_V(1), d_V(2), \dots, d_V(N)$ are randomly selected. n_H and n_L are the refractive indices of the high-index scatterers and the low-index host material. L is the length of the cylindrical scatterers, and D is the diameters of the cylindrical scatterers. d_H is the horizontal spacing. $d_V(1), d_V(2), d_V(3), \dots, d_V(N)$ are the vertical spacings between the scatterers.

imposed by the pre-determined index contrast ratio. Due to the layer-by-layer deposition, the control of the individual layer thickness is simple [29] for photonic crystal reflectors (PCRs), and from the fabrication point of view, periodic or aperiodic 3-D PCRs are of the same complexity. Specifically for solar cell application, the cost can be further reduced by using diffuse medium reflectors, which will be discussed in Section 5. Nonetheless, the physics of bandgap widening by aperiodicity is the same for A-PCRs, diffuse mirrors, and A-DBRs.

5. Dielectric Mirror Using a Diffuse Medium

Diffuse mirrors, such as white paint reflector [2], [3], are very promising for photovoltaics due to its low-cost, low-temperature processing, easy compatibility for roll-to-roll printing, higher throughput, and zero plasmonic absorptions. It is a promising alternative to conventional metallic back reflectors for solar cells. The common diffuse mirror structures including TiO_2 , ZnO , or Si_3N_4 scatterers embedded in SiO_2 , silica glass, or organic polymers, as illustrated in Fig. 6. In this study, the n_H is assumed to be 2.5, and n_L for the host material is assumed to be 1.5. The ultra-low cost process of white paint diffuse mirrors is extremely promising for solar cells [2], [3]. The optimized geometry of the periodic structure in Fig. 7 is $D_H = 147.1$ nm, $D_V = 108.2$ nm, $L = 103.1$ nm, and $D = 349.8$ nm. For the aperiodic structure in Fig. 7, $L = 71.3$ nm, $D = 228.9$ nm, $D_H = 25.4$ nm, and D_V is randomly distributed between 0 nm to 300 nm, similar to real diffuse mirrors. The use of cylindrical scatterers can provide wide reflection band using fewer layers of dielectric scatterers, compared to spherical scatterers. Nonetheless, using spherical scatterers can still provide very decent reflection band if the thickness of the diffuse mirror is thick enough. Previously, the analysis along the line of a spectral N flux method [17]–[19], a Monte Carlo method [16], and a 1-D approximation using semi-coherent optics [2] have been employed to analyze the diffuse mirrors, and the calculated reflectance around 80% is reported. The 80% reflectance, however, is lower than the experimentally reported reflectance that can be close to unity. In Fig. 7, it is shown that the reflectance of a diffuse medium reflector

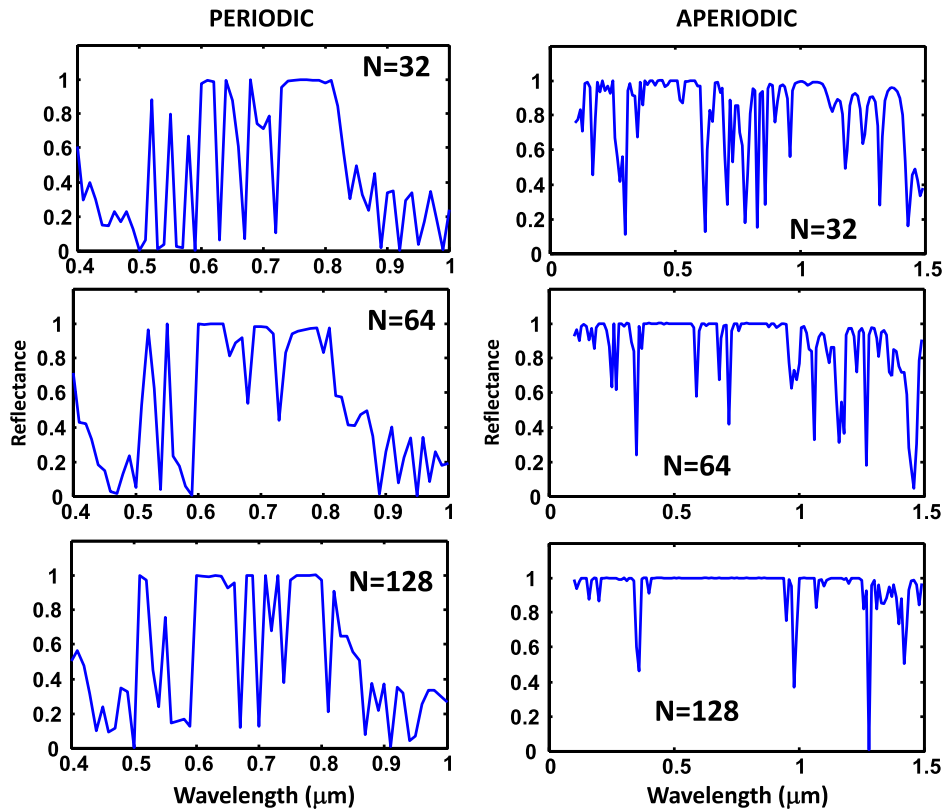


Fig. 7. Spectral reflectance of diffuse medium reflectors. (Left) Periodic stacking. (Right) Aperiodic stacking. N is the number of pairs. The length of the cylindrical scatterers (L), the diameters of the cylindrical scatterers (D), and the horizontal spacing d_H is optimized by GA. Vertical spacing between scatterers d_V is chosen randomly.

can be as high as $> 99\%$ in its reflection band, provided that the scatterer geometry is properly optimized. This reflects the improved accuracy of wave optics modeling employed in this section.

For the most recent work in literature based on 1-D approximation using semi-coherent optics [2], the 3-D dielectric scattering is approximated by one-dimensional layers. In our work, the calculation is further improved where the randomness in propagation directions (z -direction) is retained, and the three-dimensional Mie scattering initiated by embedded dielectric scatterers is accurately described by wave optics. The slight discrepancy from the real diffuse mirror is that the scatterers still distributed periodically in the x - and y -directions. Nonetheless, the randomness in x - and y -direction will only further increase the reflection band, based on a comparison between periodically and randomly distributed scatterers in the z -direction (see Fig. 7). Furthermore, the distribution of scatterer position in x - and y -direction has less effect than the distribution in z -direction since the z -direction is the primary wave propagation/incident direction.

Similar to A-PCR in Section 4, the reflection band for periodically distributed scatterers in a diffuse mirror is quite limited, as can be seen in Fig. 7. The periodically arranged scatterers can be achieved by some reported solution processes where the alignment of dielectric scatterers embedded in organic polymers is accomplished [14], [15]. In Fig. 7, the reflection band for randomly distributed scatterers embedded in low-index host materials is much wider. The reflection band can be further increased by including more scattering layers, and this is also illustrated in Fig. 7 for different N . It should be pointed out that increasing the thickness of a diffuse mirror, such as a white paint reflector, does not increase the cost. This is due to that fact that the exactly same solution process can be used for the white paint reflectors of different thicknesses, and the raw material is relatively cheap. The aperiodic design with accurately designed vertical

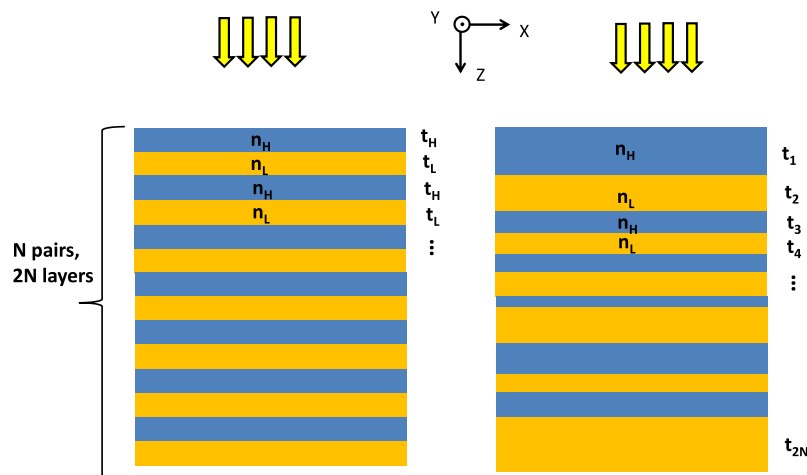


Fig. 8. Periodic and aperiodic distributed Bragg reflector (DBR) stacking. n_H and t_H are the refractive index and the thickness of the high index material. n_L and t_L are the refractive index and the thickness of the low index material. In the case of aperiodic stacks, the thickness is different for each layer, and it is denoted by t_1, t_2, t_3, \dots , or t_{2N} . t_1, t_2, \dots, t_{2N} are independently chosen. The optimization of the A-DBR can be referred to Section 2.

spacing (D_v) between each layer is also possible computationally, which is termed optimized aperiodicity similar to the case of A-PCRs. Based on our study, an even wider reflection band can be achieved due to the optimized D_v . Nonetheless, since in real diffuse mirrors, accurately controlled scatterer spacing is more difficult to realize, the randomly distributed scatterers are used here to study the effect of aperiodicity. It should be pointed out that both accurately controlled aperiodic structures and randomly distributed structures fall into the category of aperiodic designs. The physics behind the widened reflection band of a diffuse mirror, with increased aperiodic stacking thickness, is still photonic bandgap widening, and this has been explained in detail in Section 3.

6. Aperiodic Distributed Bragg Reflector (A-DBR)

Finally, the most common one-dimensional distributed Bragg reflectors (DBR) is examined as illustrated in Fig. 8. It is found that the same physics and design principle can be applied to DBR structures. The optimized geometry for periodic DBR is trivially quarter-wavelengths with the center wavelength chosen as 400 nm in this study. For the aperiodic DBRs (A-DBR), the individual layer thickness is varying between 0 nm to one wavelength. The layer thicknesses can be systematically optimized by optimization algorithms, but this is not necessary since the planar structure is simpler to design and to select proper geometry. The practice here is iteratively running potential A-DBR candidates with randomly chosen layer thickness. Widest reflection band individual is selected for the demonstration in Fig. 9. For the periodic DBR in Fig. 9, the quarter-wavelength slabs lead to constructive interferences of reflected waves for a limited spectral range. Therefore, the reflection band only spans 132 nm, and outside the reflection band the interference condition rapidly diminishes. It has been known for a long time that increasing the number of DBR pairs, for a fixed index contrast ratio, does not help to widen the reflection bandwidth. Increasing pair number N only sharpens the response, as evident from Fig. 9. The only way to increase the bandwidth is by using materials with higher index contrast if a periodic design is employed. On the contrary, it is seen in Fig. 9 that the aperiodic structures are capable of providing wider reflection band. Similar to the aperiodic photonic crystal reflectors (A-PCR) and diffuse medium mirrors in previous sections, the reflection bandwidth can be widened arbitrarily by adding more aperiodically stacked layers. The bandwidth widening phenomenon is clearly illustrated in Fig. 9.

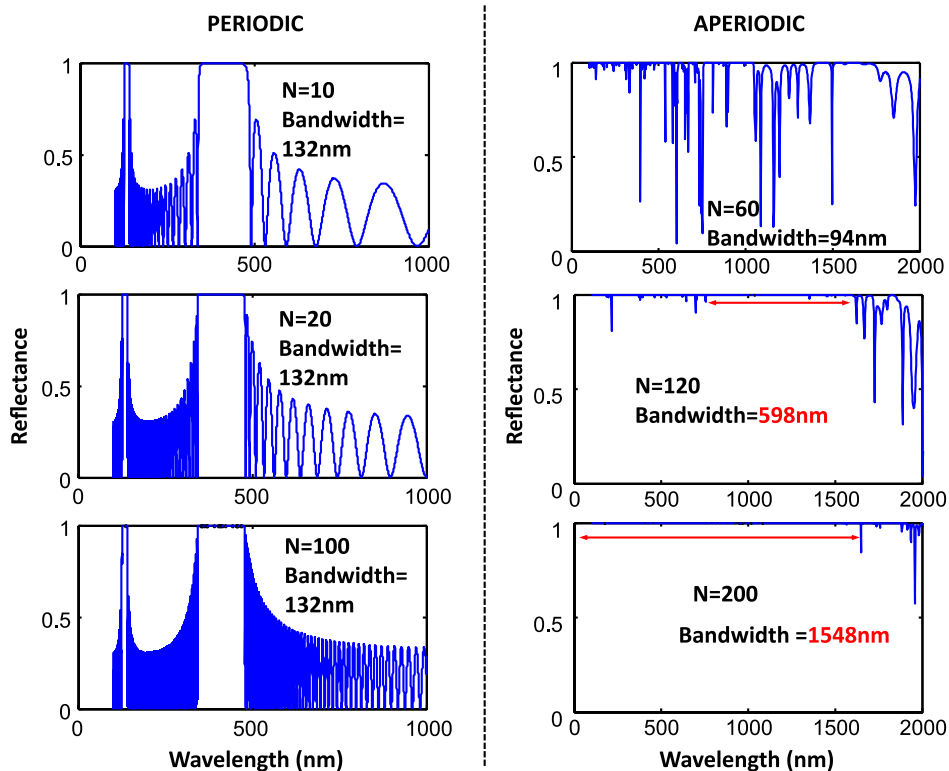


Fig. 9. Spectral reflectance of DBR mirrors. (Left) Periodic stacking. (Right) Aperiodic stacking. N is the number of pairs.

7. Experimental Verification Using Diffuse Medium Reflectors and SiGe Solar Cells

The experimental demonstration of diffuse medium white-paint reflectors is included in this section. The commercial white paint is mostly made of pigments and a binder material. The pigments are nanoparticles with size ranging from 200 nm–500 nm, and the binder is a lower-index material. Three different white-paint materials are tested in this paper. One is a commercial white-out, and the other two are household white paints. The commercial Pantel white-out is employed in this work. On the other hand, the white paint 1 consists of unspecified pigments embedded in synthetic resin and the white paint 2 consists of TiO_2 nanoparticles embedded in synthetic resin. The high reflectance over a broad spectral range is verified by ultra-violet visible spectroscopy (UV–VIS) measurement, and it can be seen that the full spectral range for solar cell application is easily achieved by using white-paint diffuse medium reflectors with randomly distributed nanoparticles. The fabrication of silicon germanium (SiGe) thin-film solar cell is conducted using very high-frequency plasma enhanced chemical vapor deposition (VHF-PECVD). Fluorine-doped tin oxide (FTO) coated glass is firstly cleaned by acetone. Afterward, the p-i-n amorphous silicon-germanium (α -SiGe) film is deposited on FTO coated glass. The thickness of p-type α -Si, intrinsic α -Si, intrinsic α -SiGe and n-type α -Si layers are 8 nm, 10 nm, 175 nm, and 20 nm, respectively. The p-i-n silicon-germanium film is deposited by very-high-frequency plasma-enhanced chemical vapor deposition (VHF-PECVD) at 300 °C. Finally, the indium tin oxide (ITO) thickness is 200 nm and is deposited by sputtering. A shadow mask is placed on top of the n-type α -Si layer during ITO deposition, to form the patterned ITO electrodes. Since the white paint material currently used in this study is non-conducting, etching is necessary to make ohmic contacts to the bottom FTO layer which is in turn in contact with the p-type emitter. Reactive ion etching (RIE) using CF_4 /Argon (Ar) at 20 mtorr is employed to etch the portion of SiGe

Baseline:

$$V_{oc} = 0.56 \text{ V}, J_{sc} = 10.25 \text{ mA/cm}^2, \eta = 1.79$$

White Paint:

$$V_{oc} = 0.57 \text{ V}, J_{sc} = 12.07 \text{ mA/cm}^2, \eta = 2.29$$

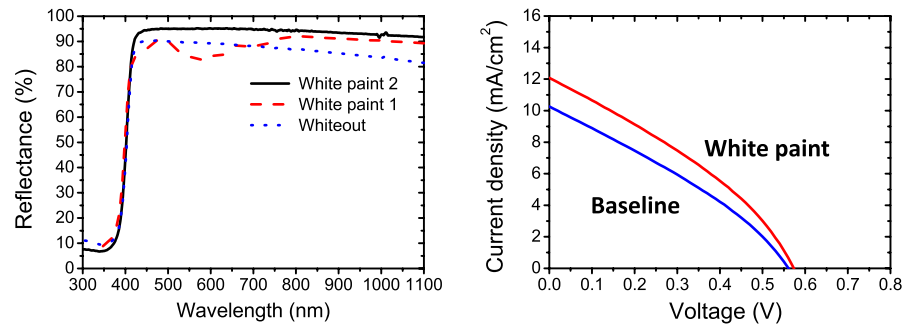


Fig. 10. Experimental demonstration of the random diffuse medium reflectors and its application to SiGe thin-film solar cell. The structure consists of glass, fluorine tin oxide (FTO), amorphous silicon (α -Si) and amorphous silicon germanium (α -SiGe), and indium tin oxide (ITO). V_{oc} is open-circuit voltage; J_{sc} is short-circuit current density; and η is the conversion efficiency of solar cells. The light is incident from the ITO side.

film which is not covered with indium tin oxide (ITO), and thus, the contact to the bottom FTO layer is achieved. From Fig. 10, the feasibility of a diffuse medium reflector is confirmed, and the efficiency of α -SiGe solar cell is improved by 27% by applying a broadband white paint diffuse medium reflector.

8. Conclusion

The ultra-wideband dielectric mirrors are proposed based on aperiodic stacking. The reflection bandwidth can be increased for a fixed index contrast ratio, by incorporating more dielectric layers. Incorporating more dielectric layers can be achieved at no extra cost for diffuse medium mirrors since this can be done by simply increasing the thickness of the white paint. Widened reflection band is unachievable in any periodic designs since increasing the deposited pairs only sharpens the spectral response of a periodic structure. The phenomenon of the reflection bandwidth widening through aperiodic stacking is well-applied to many dielectric mirror configurations including aperiodic photonic crystal reflectors (A-PCR), diffuse medium mirrors, and aperiodic distributed Bragg reflectors (A-DBR). Based on the photonic bandstructure calculation, the physics behind widened reflection bandwidth is identified as the photonic band-gap widening due to the annihilation of quasi-guided modes in the non-periodic dielectric mirror structures. Specifically, the reduced resonance strength by the aperiodic design will cause the disappearance of reflection dips, and, therefore, lead to the widened reflection band in the spectrum. It is believed that aperiodically-designed dielectric mirrors will be very promising for future optoelectronic and photonic applications due to their wider bandwidth relative to their periodic counterparts, easy scalability, no plasmonic absorption, and achieving wider reflection band for a fixed index contrast ratio by simply using more aperiodic stacking layers. The experimental demonstration using SiGe solar cells with diffuse medium reflectors is included. The UV-VIS measurement shows high reflectance over a broad spectral range. The enhancement of solar cell efficiency by incorporating low-cost dielectric mirrors is also very pronounced.

Acknowledgment

The authors wish to thank the anonymous reviewers for their valuable suggestions. They also wish to thank Prof. P. Yu for the fruitful discussion and for help with the ultra-violet visible spectroscopy (UV-VIS) measurement.

References

- [1] P. Bhattacharya, *Semiconductor Optoelectronic Devices*, 2nd Ed. Upper Saddle River, NJ, USA: Prentice-Hall, 2006.
- [2] B. Lipovšek, J. Krč, O. Isabella, M. Zeman, and M. Topič, "Modeling and optimization of white paint back reflectors for thin-film silicon solar cells," *J. Appl. Phys.*, vol. 108, no. 10, 2010, Art. ID. 103115.
- [3] S. Hänni *et al.*, "High-efficiency microcrystalline silicon single-junction solar cells," *Prog. Photovolt: Res. Appl.*, vol. 21, no. 5, pp. 821–826, Aug. 2013.
- [4] M. C. Y. Huang, Y. Zhou, and C. J. Chang-Hasnain, "A nanoelectromechanical tunable laser," *Nat. Photon.*, vol. 2, pp. 180–184, 2008.
- [5] X. M. Zhang *et al.*, "Variable nano-grating for tunable filters," in *Proc. 14th Int. Conf. Solid-State Sens., Actuators Microsyst.*, Lyon, France, 2007, pp. 2417–2420.
- [6] V. Karagodsky, Forrest G. Sedgwick, and C. J. Chang-Hasnain, "Theoretical analysis of subwavelength high contrast grating reflectors," *Opt. Exp.*, vol. 18, no. 16, pp. 16 973–16 988, 2012.
- [7] V. Karagodsky and C. J. Chang-Hasnain, "Physics of near-wavelength high contrast gratings," *Opt. Exp.*, vol. 20, pp. 10 888–10 895, 2012.
- [8] R. G. Mote, S. F. Yu, W. Zhou, and X. F. Li, "Design and analysis of two-dimensional high index-contrast grating surface-emitting lasers," *Opt. Exp.*, vol. 17, no. 1, pp. 260–265, Jan. 2009.
- [9] R. Magnusson and M. Shokooh-Saremi, "Physical basis for wideband resonant reflectors," *Opt. Exp.*, vol. 16, no. 5, pp. 2456–3462, Mar. 2008.
- [10] S. L. Chuang, *Physics of Photonic Devices (Wiley Series in Pure and Applied Optics)*, 2nd ed. New York, NY, USA: Wiley, 2009.
- [11] C. F. R. Mateus, M. C. Y. Huang, Y. Deng, A. R. Neureuther, and C. J. Chang-Hasnain, "Ultrabroadband mirror using low-index cladded subwavelength grating," *IEEE Photon. Tech. Lett.*, vol. 16, no. 2, pp. 518–520, Feb. 2004.
- [12] J. Foley, S. Young, and J. Phillips, "Symmetry-protected mode coupling near normal incidence for narrow-band transmission filtering in a dielectric grating," *Phys. Rev. B, Condens. Matter*, vol. 89, no. 16, Apr. 2014, Art. ID. 165111.
- [13] J. M. Foley, A. M. Itsuno, T. Das, S. Velicu, and J. D. Phillips, "Broadband long-wavelength infrared Si/SiO₂ subwavelength grating reflector," *Opt. Lett.*, vol. 37, no. 9, pp. 1523–1525, May 2012.
- [14] C. Y. Kuo, W. C. Tang, C. Gau, T. F. Guo, and D. Z. Jeng, "Ordered bulk heterojunction solar cells with vertically aligned TiO₂ nanorods embedded in a conjugated polymer," *Appl. Phys. Lett.*, vol. 93, no. 3, 2008, Art. ID. 033307.
- [15] Y. Han, C. Fan, G. Wu, H.-Z. Chen, and M. Wang, "Low-temperature solution processed ultraviolet photodetector based on an ordered TiO₂ nanorod array-polymer hybrid," *J. Phys. Chem. C*, vol. 115, no. 27, pp. 13 438–13 445, 2011.
- [16] P. Nitz, J. Ferber, R. Stangl, H. R. Wilson, and V. Wittwer, "Simulation of multiply scattering media," *Solar. Energy. Mater. Solar Cells*, vol. 54, no. 1–4, pp. 297–307, Jul. 1998.
- [17] W. E. Vargas, A. Amador, and G. A. Niklasson, "Diffuse reflectance of TiO₂ pigmented paints: Spectral dependence of the average pathlength parameter and the forward scattering ratio," *Opt. Commun.*, vol. 261, no. 1, pp. 71–78, May 2006.
- [18] W. E. Vargas, P. Greenwood, J. E. Otterstedt, and G. A. Niklasson, "Light scattering in pigmented coatings: Experiment and theory," *Solar Energy*, vol. 68, no. 6, pp. 553–561, 2000.
- [19] J. E. Cotter, "Optical intensity of light in layers of silicon with rear diffuse reflectors," *J. Appl. Phys.*, vol. 84, no. 1, pp. 618–624, 1998.
- [20] A. Chipperfield, P. Fleming, H. Pohlheim, and C. Fonseca, *Genetic Algorithm Toolbox User Guide*. Sheffield, U.K.: Univ. Sheffield, 1994.
- [21] B. Deken, S. Pekarek, and F. Dogan, "Minimization of field enhancement in multilayer capacitors," *Comput. Mater. Sci.*, vol. 37, no. 3, pp. 401–409, 2006.
- [22] S. Preblea, M. Lipson, and H. Lipson, "Two-dimensional photonic crystals designed by evolutionary algorithms," *Appl. Phys. Lett.*, vol. 86, no. 6, 2005, Art. ID. 061111.
- [23] L. Shen, Z. Ye, and S. He, "Design of two-dimensional photonic crystals with large absolute band gaps using a genetic algorithm," *Phys. Rev. B, Condens. Matter*, vol. 68, no. 3, Jul. 2003, Art. ID. 035109.
- [24] H. Lipson and J. B. Pollack, "Automatic design and manufacture of robotic lifeforms," *Nature*, vol. 406, pp. 974–978, Aug. 2000.
- [25] J. D. Joannopoulos, S. G. Johnson, R. D. Meade, and J. N. Winn, *Photonic Crystal: Molding the Flow of Light*, 2nd ed. Princeton, NJ, USA: Princeton Univ. Press, 2008.
- [26] C. Battaglia *et al.*, "Light trapping in solar cells: Can periodic beat random?" *ACS Nano.*, vol. 6, no. 3, pp. 2790–2797, Mar. 2012.
- [27] A. S. Lin *et al.*, "Lithographically fabricable, optimized three-dimensional solar cell random structure," *J. Opt.*, vol. 15, no. 10, Oct. 2013, Art. ID. 105007.
- [28] C.-Y. Huang, H.-M. Ku, and S. Chao, "Light extraction enhancement for InGaN/GaN LED by three dimensional auto-cloned photonics crystal," *Opt. Exp.*, vol. 17, no. 26, pp. 23 702–23 711, Dec. 2009.
- [29] Y. Ohtera and H. Yamada, "Multichannel bandpass filters utilizing multilayer photonic crystal," *Opt. Lett.*, vol. 38, no. 8, pp. 1235–1237, Apr. 2013.